

Article

Effect of Laser Peening on the Corrosion Properties of 304L Stainless Steel

Young-Ran Yoo ^{1,*}, Seung-Heon Choi ^{1,2} and Young-Sik Kim ^{1,2,*}

¹ Materials Research Centre for Energy and Clean Technology, Andong National University, 1375 Gyeongdong-ro, Andong 36729, Republic of Korea

² School of Materials Science and Engineering, Andong National University, 1375 Gyeongdong-ro, Andong 36729, Republic of Korea

* Correspondence: yryoo@anu.ac.kr (Y.-R.Y.); yikim@anu.ac.kr (Y.-S.K.);
Tel.: +82-54-820-7897 (Y.-R.Y.); +82-54-820-5504 (Y.-S.K.)

Abstract: Dry canisters used in nuclear power plants can be subject to localized corrosion, including stress corrosion cracking. External and residual tensile stress can facilitate the occurrence of stress corrosion cracking. Residual stress can arise from welding and plastic deformation. Mitigation methods of residual stress depend upon the energy used and include laser peening, ultrasonic peening, ultrasonic nanocrystal surface modification, shot peening, or water jet peening. Among these, laser peening technology irradiates a continuous laser beam on the surface of metals and alloys at short intervals to add compressive residual stress as a shock wave is caused. This research studied the effect of laser peening with/without a thin aluminum layer on the corrosion properties of welded 304L stainless steel. The intergranular corrosion rate of the laser-peened specimen was a little faster than the rate of the non-peened specimen. However, laser peening enhanced the polarization properties of the cross-section of 304L stainless steel, while the properties of the surface were reduced by laser peening. This behavior was discussed on the basis of the microstructure and residual stress.

Keywords: laser peening; stainless steel; passivation; intergranular corrosion; cross-section



Citation: Yoo, Y.-R.; Choi, S.-H.; Kim, Y.-S. Effect of Laser Peening on the Corrosion Properties of 304L Stainless Steel. *Materials* **2023**, *16*, 804. <https://doi.org/10.3390/ma16020804>

Academic Editors: Yujie Qiang and You Zhang

Received: 23 November 2022

Revised: 30 December 2022

Accepted: 11 January 2023

Published: 13 January 2023



Copyright: © 2023 by the authors. Licensee MDPI, Basel, Switzerland. This article is an open access article distributed under the terms and conditions of the Creative Commons Attribution (CC BY) license (<https://creativecommons.org/licenses/by/4.0/>).

1. Introduction

When metals and alloys are stressed beyond their elastic limits, they can be plastically deformed, and residual stress remains on metals and alloys. There are three reasons for this stress forming: When metals and alloys are cooled from a high temperature, there is often a thermal difference during cooling. The varying thermal difference develops non-uniform stress. In addition, phase transformation and mechanical processing can induce residual stress in metals and alloys. This residual stress facilitates the cracking and corrosion of metals and alloys. High residual stress can be generated near weldment due to the non-uniform thermal gradient formed from localized faster heating and cooling during the welding process [1,2].

Generally, mitigation methods for residual stress include post-welding heat treatment, low-temperature stress relief, mechanical stress relief, and surface modification methods. Of these methods, surface modification methods depend upon the energy used and include laser peening [3], ultrasonic peening [4], ultrasonic nanocrystal surface modification [5], shot peening [6], and water jet peening [7].

Laser peening is a technology that irradiates a continuous laser beam on the surface of metals and alloys at short intervals to add compressive residual stress as a shock wave is caused [8]. When laser peening is performed, plasma is concentrated on the surface using a transparent overlay (water [9] or glass [10] layer), and absorption layers (Al [11,12], vinyl tape [13,14]) are used to form effective compressive residual stress. When laser peening is performed by positioning an absorption layer that maintains the high quality of the surface and effectively maintains surface melting and energy conversion, compressive residual

stress is formed [15] and grain refinement occurs [16], which leads to microstructural changes due to increasing dislocation density and strain [17]. This influences intergranular corrosion, corrosion fatigue, and SCC properties. We recently reported the effect of laser peening on the microstructure of 304L stainless steel: Laser peening resulted in the increased roughness of the surface, refinement of the grain size, deformation of the inside, increased dislocation density, and increased hardness of 304L stainless steel [18].

Corrosion properties by surface modification have recently been studied as follows: Shot peening on the corrosion of aluminum alloy [19,20] and the corrosion properties of stainless steel [21,22]; laser peening on the corrosion of Alloy 600 [23], the corrosion of 304 stainless steel [24], the corrosion of stainless steels [25–29], the corrosion of aluminum alloy [30], and the corrosion of magnesium alloy [31]; UNSM on the corrosion of nickel base alloys [32–34] and the corrosion of stainless steels [35–38]; and comparison between laser peening, shot peening, and ultrasonic peening [8]. Most recent research efforts on surface modification methods have shown beneficial effects on the corrosion of various alloys [19–38]. In some cases, detrimental effects of surface modification methods can be induced. For example, a high static load can degrade corrosion resistance [34]. According to a recent report by our group, ultrasonic nanocrystal surface modification increases corrosion resistance, but beyond the critical static load, corrosion resistance decreases as the repeated striking of the surface creates an overlapped wave which acts as the initiation site of corrosion [34]. As described above, surface modification methods including laser peening increase corrosion properties in some cases, but degrade resistance in other cases. That is, it is not clear how surface modification affects corrosion resistance.

In this study, we made laser-peened 304L stainless steel, which has a compressive residual stress of over 1 mm, evaluated intergranular corrosion properties and polarization behavior, and measured residual stress. Resistances were discussed and the effect of laser peening on corrosion properties was elucidated.

2. Experimental Methods

2.1. Specimen

The specimen used in this work was commercial 304L stainless steel; Table 1 shows the chemical composition of 304L stainless steel and its filler metal [18]. The thickness of the specimen was 25 mm. The specimen was welded using the gas tungsten arc welding (GTAW) method by the following conditions (see Table 2) [18]. Table 3 shows the designation of the specimen's condition [18].

Table 1. Chemical composition of 304L stainless steel and filler metal (wt %) [18].

	C	Cr	Ni	Mn	Si	Cu	Mo	Co	P	N	S	Cb + Ta	Fe
304L	0.02	18.6	9.6	1.65	0.47	-	-	0.03	0.022	0.07	0.03	-	Bal.
ER308L	0.015	19.81	9.84	1.691	0.351	0.115	0.046	0.030	0.024	0.041	0.03	0.008	Bal.

Table 2. Welding conditions of the experimental specimen [18].

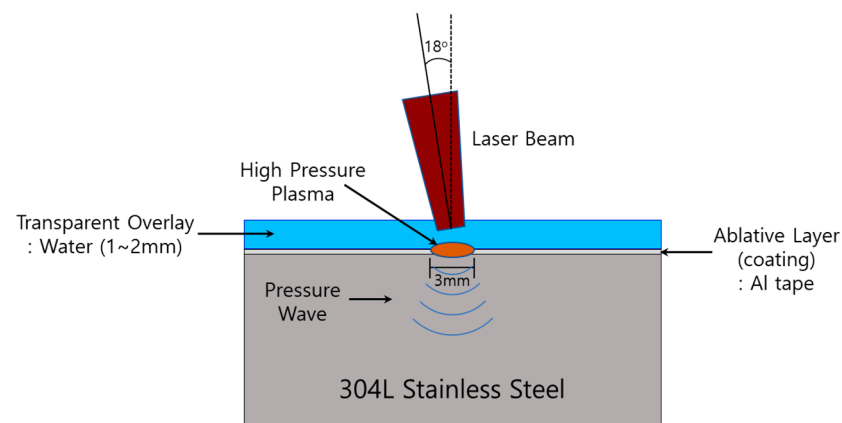
Welding Process	Current (A)	Voltage (V)	Speed (cm/min)	Shield Gas (%)	Groove Angle (°)	Welding Electrode
GTAW	245~250	14~15	9~10	Ar. 99.9	15	ER308L (Dia. 0.9 mm wire)

Table 3. Designation of the experimental specimen [18].

	Alloy	Non-Peened	Laser Peening	
			Non-Coated	With Coating
304L	Base metal	304LB	304LB-L-NC	304LB-L-WC
	HAZ area	304LW-H	304LW-H-L-NC	304LW-H-L-WC
	Weldment	304LW-W	304LW-W-L-NC	304LW-W-L-WC

2.2. Laser Peening (LP)

The laser peening process employed in this study was well described elsewhere: Figure 1 shows the schematic diagram of laser peening and Table 4 summarizes the laser peening conditions [18]. The equipment for laser peening was self-manufactured using an Nd-YAG laser to protect the steel's surface during the laser peening process and Al tape was used. The laser energy used was 4.4 J and a water layer of 1~2 mm was dynamically overlaid. The laser incident beam angle was 18°.

**Figure 1.** Schematic of laser peening process [18].**Table 4.** Conditions of laser peening treatment [18].

Laser Type	Laser Energy (J)	Laser Spot Diameter (mm)	Laser Overlay (%)	Transparent Overlay	Laser Incident Beam Angle (°)	Coating
Nd-YAG (1064 nm, IR)	4.4	3	50	Water (1~2 mm)	18	Al tape

2.3. Qualitative Degree of Sensitization Measurement: ASTM A262 Pr. A

The specimens were cut to sizes of 15 × 15 × 10 mm. They were connected to an insulated electrical lead wire and mounted using an epoxy. Then, the cross-section of the specimen was prepared through grinding and polishing using #2000 SiC paper and diamond paste (3 μm), respectively. Specimens were insulated with a resin, except for an area of 1 cm². The specimen was anodically dissolved for 90 s at 1 A/cm² in 10% oxalic acid. After ultrasonic cleaning, the sample was observed using an optical microscope and the degree of sensitization was determined as shown in the standard [39].

2.4. Quantitative Degree of Sensitization Measurement: DL-EPR Test

The specimens were cut to sizes of 15 × 15 × 10 mm. They were connected to an insulated electrical lead wire and mounted using an epoxy. Then, the cross-section of the specimen was prepared through grinding and polishing using #2000 SiC paper and diamond paste (3 μm), respectively. The polished cross-section, except for an area of

0.09 cm², was electrically insulated with a resin. According to ASTM G108, a double loop-electrochemical potentiokinetic reactivation (DL-EPR) test was performed [40]. The test solution was 0.5 M H₂SO₄ + 0.01 M KSCN at 30 °C and was deaerated at a rate of 200 mL N₂/min for 30 min. A DL-EPR test was performed using a potentiostat (Interface 1000, Gamry Instruments, Warminster, PA, USA). Pt wire and a saturated calomel electrode were used as the counter and reference electrodes, respectively. Anodic scan to vertex potential (+400 mV(SCE)) and reactivation were swept, and the scan rate was at a rate of 1.677 mV/s. According to the standard [39], the ratio of I_r/I_a was determined, indicating the degree of sensitization (DOS).

After the test, the specimen was taken out and ultrasonically cleaned, and the cross-section was observed using an optical microscope (AXIOTECH 100 HD, ZEISS, Oberkochen, Germany).

2.5. Intergranular Corrosion Rate Measurement: ASTM A262 Pr. C

The specimens were cut to sizes of 15 × 15 × 10 mm and aged for 1 h at 675 °C. Then, the specimen, except the peened surface, was ground using SiC paper from #120 to #2000. An immersion test in 65% HNO₃ at boiling temperature was performed according to ASTM A262 Pr. C [39]; each test time took 3 h due to the possibility of severe corrosion on the peened surface. The tests were repeated five times. The intergranular corrosion rate was obtained from the weight loss and intergranular corrosion was confirmed by field emission-SEM (MIRA3 XMH, Tescan, Brno, Czech Republic) of the corroded cross-section.

2.6. Anodic Polarization Test

The specimens were cut to sizes of 15 × 15 × 10 mm. The specimens were connected to an insulated electrical lead wire. The non-peened specimen was mounted using an epoxy and ground using #2000 SiC paper, but the peened specimen was insulated with an epoxy resin. An area of 0.09 cm² was exposed to a test solution. A potentiostat (Interface 1000, Gamry Instruments, Warminster, PA, USA) was used and a saturated calomel electrode for the reference electrode and Pt wire for the counter electrode were used. The test solution was 1% NaCl at 30 °C and deaerated at a rate of 200 mL N₂/min for 30 min. After the specimen was immersed into Avesta cell, it was cathodically polarized at −200 mV from open circuit potential for 10 min to remove the surface oxide and then maintained at open circuit potential for 10 min. After the corrosion potential was measured, the polarization curve was obtained from −100 mV than the corrosion potential. The scan rate was 0.33 mV/s [41].

2.7. AC Impedance Test

The specimens were cut to sizes of 15 × 15 × 10 mm. The specimen and potentiostat used were the same as with the anodic polarization test. The test solution was 1% NaCl at 30 °C and deaerated at a rate of 200 mL N₂/min for 30 min. The frequency range was 0.01~10,000 Hz, and an AC impedance test was performed at the corrosion potential. Polarization resistance was calculated using an equivalent circuit of Randles model [42].

2.8. Residual Stress Measurement

The residual stress was performed via a hole drilling method (RS-200 Assembly, VMM, USA). A strain gauge was attached and holes were fabricated by using a drilling device. The residual stresses released during the drilling were measured.

3. Results and Discussion

3.1. Effect of Laser Peening on the Intergranular Corrosion of 304L Stainless Steel

Figure 2 shows the effect of laser peening on intergranular corrosion by ASTM A262 Pr. A [39] for the outermost area of the cross-section of base metal, HAZ (heat affected zone), and weldment of 304L stainless steel. In the case of the base metal, the grain boundaries looked like the etched microstructure. In the case of the heat-affected zone, the grains were

grown, and the grain boundaries also looked like the etched microstructure. However, in the case of weldment, a dendritic structure was observed, and the dendrite grew along the direction in which heat escapes. Compared to the sensitization of the base metal, the effect of laser peening on the sensitization of the cross-section of 304L stainless steel was slight, but the outermost area by laser peening showed a refined microstructure and more corrosion, regardless of the area.

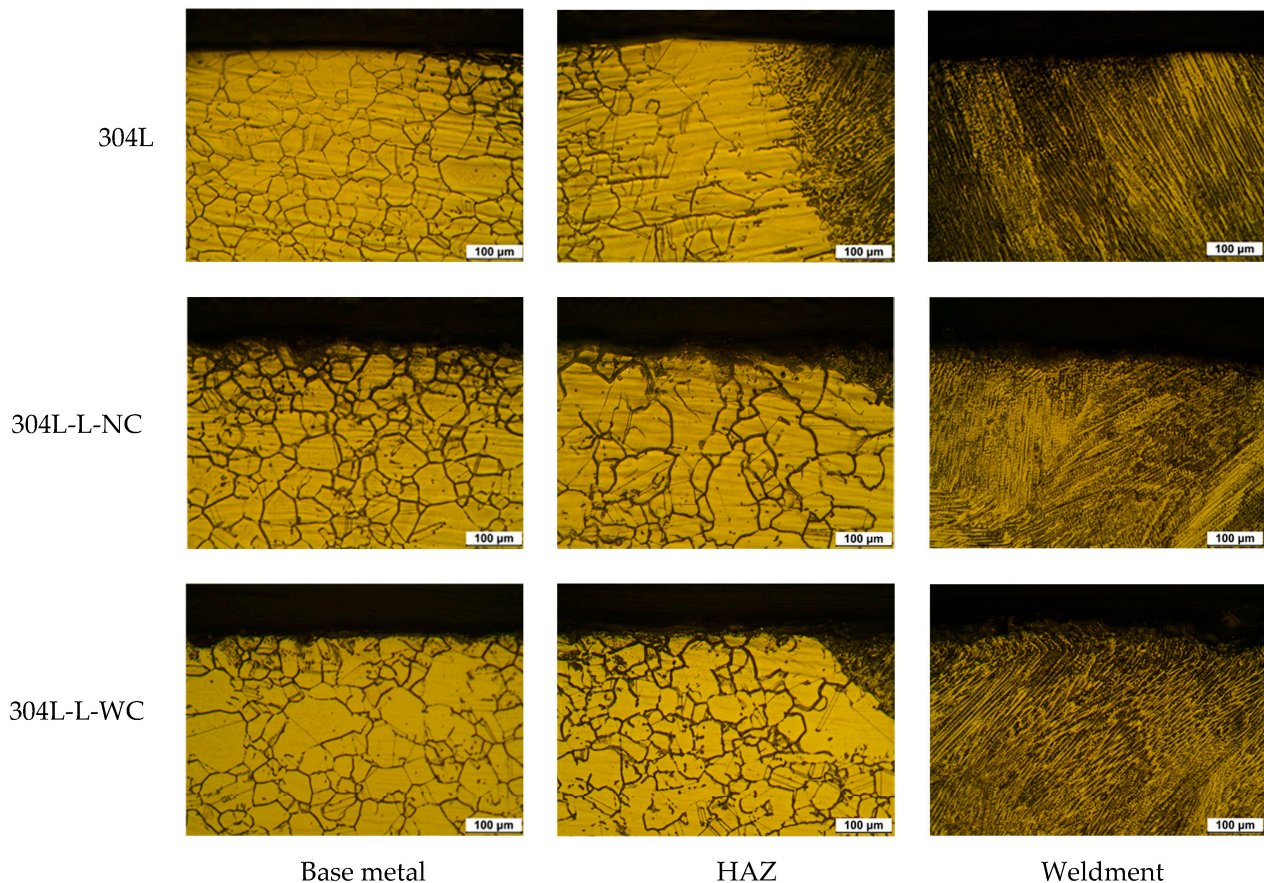


Figure 2. Effect of laser peening on the degree of sensitization obtained by ASTM A262 Pr. A for the outermost area of the cross-section of 304L stainless steel (OM, $\times 200$).

Figure 3 shows the effect of laser peening on the average grain size by ASTM E1382 [43]. Figure 3a shows the base metal, while Figure 3b shows the HAZ area. The average grain size was measured three times and the standard deviation was calculated. Regardless of the observed area, the laser peening treatment refined the grain size. These refinements were due to the outermost area of the laser peening. However, the average grain size of the HAZ area was greater than the size of the base metal, regardless of the peening condition. When the laser peening was forced to the surface, the grain size of the outermost area was refined, and this refinement yielded a partly smaller grain size for the observed area. Note that the refinement of the outermost area needed to be much more intensive than that of the observed area [18]. In addition, the average grain size of the HAZ area was greater than the size of the base metal due to the grain growth of the HAZ area by welding.

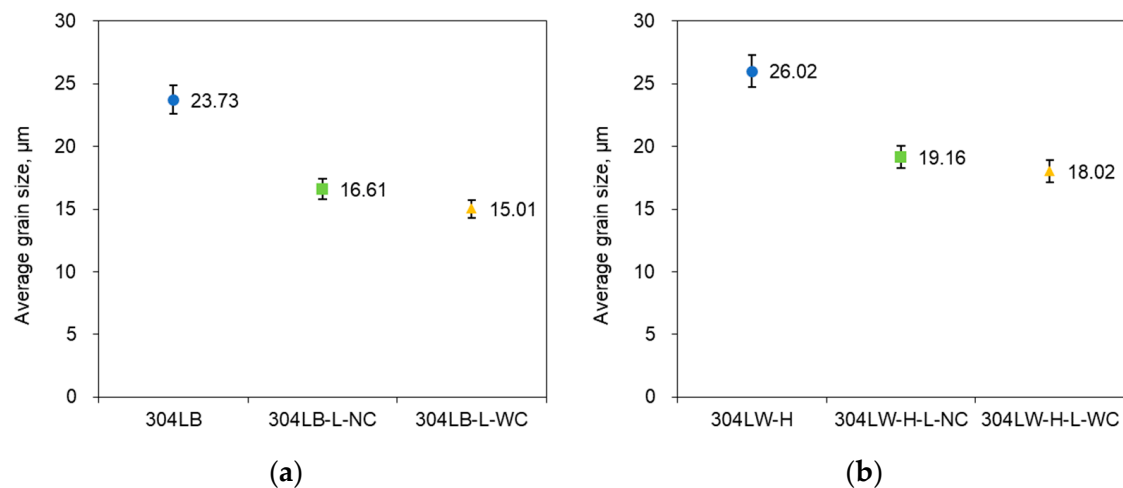


Figure 3. Effect of laser peening on grain size by ASTM E1382; (a) Base metal, (b) HAZ area.

Figure 4 shows the effect of laser peening on the DL-EPR curve and DOS of the outermost area of the cross-section of 304L by a double loop-electrochemical potentiokinetic reactivation test. The DOS of base metal 304LB was 0.00003, but that of 304LB peened by laser without Al coating was 0.00641, while that of 304LB peened by laser with Al coating was 0.0002. That is, laser peening increased the degree of sensitization. The DOS of the HAZ area of 304LW was 0.00095, but that of the HAZ area of 304LW peened by laser without Al coating was 0.00735, while that of the HAZ area of 304LW peened by laser with Al coating was 0.00316. That is, laser peening also increased sensitization. The DOS of the weldment area of 304LW was 0.00104, but that of the weldment area of 304LW peened by laser without Al coating was 0.00614, while that of the weldment area of 304LW peened by laser with Al coating was 0.00285. That is, laser peening also increased the degree of sensitization. This behavior was due to the increased grain boundary area by the laser peening and showed a similar trend to those of the qualitative degree of sensitization, as shown in Figure 2.

Figure 5 shows the optical micrographs of the cross-section of 304L after the DL-EPR test. Compared to the photos of the base metal, the DL-EPR test corroded the outmost area of the laser-peened cross-section relatively more. However, the effects of Al-coating on the laser peening process were difficult to differentiate from each other.

Figure 6 shows the effect of laser peening on the intergranular corrosion rate of 304L obtained from the immersion test in boiling 65% HNO₃ [39]. The maximum allowable corrosion rate was referred from ISO 12732 [44]. Figure 6a shows that laser peening treatment of the base metal increased the intergranular corrosion rate, regardless of Al coating. These increased results were similar to those of the qualitative intergranular corrosion test in Figure 2 and the quantitative intergranular test in Figure 4. Figure 6b shows that laser peening treatment of the welded specimen also increased the intergranular corrosion rate, regardless of Al coating. These results were similar to those of the qualitative intergranular corrosion test in Figure 2 and the quantitative intergranular test in Figure 4. Comparing the results of the base metal and welded specimen, the welding process slightly increased the intergranular corrosion rate, but the effect of laser peening of the welded specimen was a little stronger than that of the base metal. Table 5 shows the relationship between the degree of sensitization and intergranular corrosion (IGC) rate of 304L stainless steel by laser peening. If the relationships between them, except that of 304LB-L-WC, are plotted, the trend equation is obtained as 'IGC rate, mm/y = 52.4 × (DOS) + 0.1'; its determination coefficient was calculated as 0.9919.

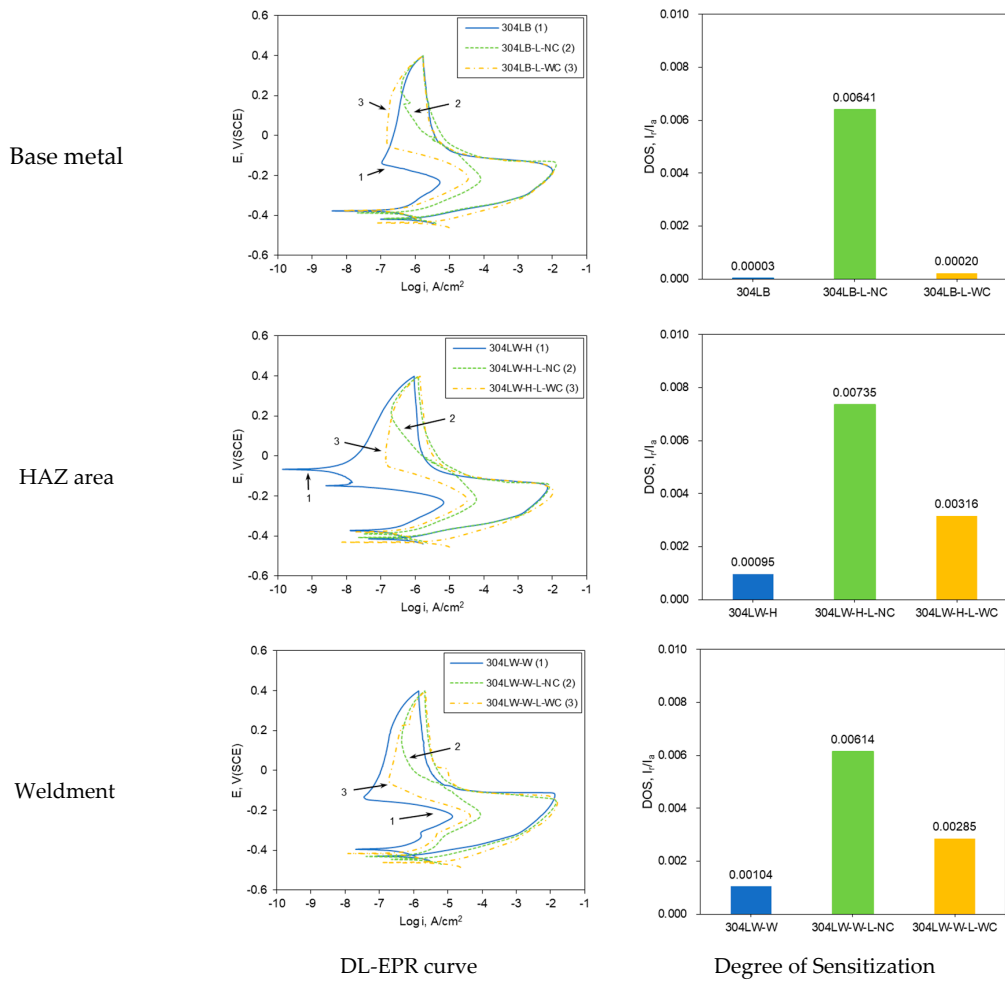


Figure 4. Effect of laser peening on the degree of sensitization on the outermost area of the cross-section of 304L by DL-EPR test.

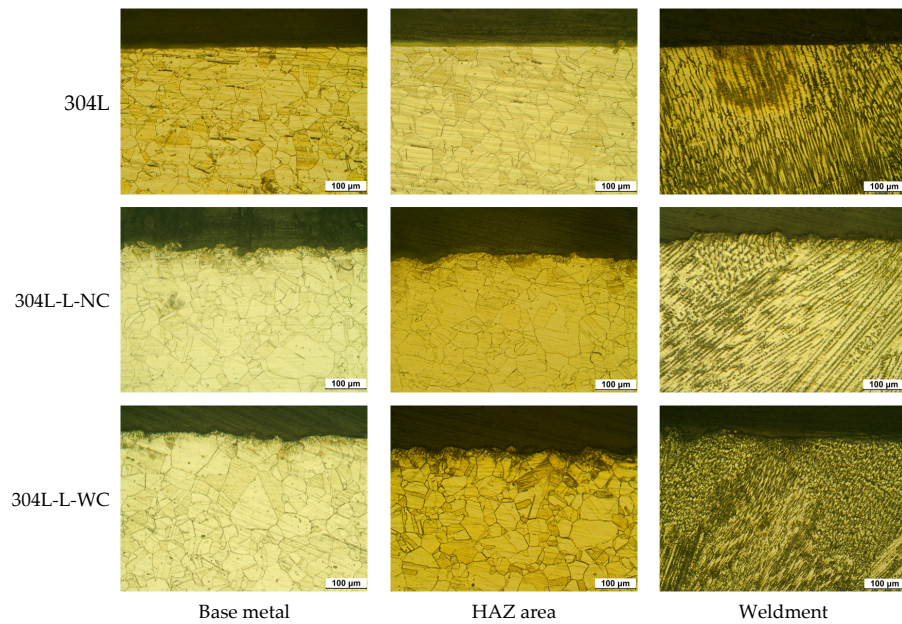


Figure 5. Cross-sectional appearance of 304L after DL-EPR test (OM, ×200).

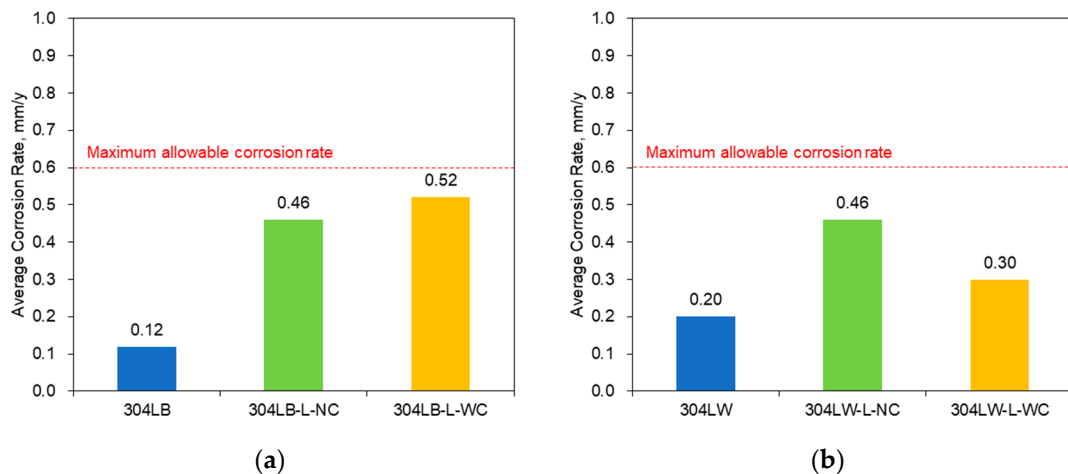


Figure 6. Effect of laser peening on the intergranular corrosion rate of 304L obtained from the immersion test in boiling 65% HNO₃; (a) Base metal, (b) Welded specimen.

Table 5. The relationship between the DOS and IGC rate of 304L stainless steel by laser peening.

	304LB	304LB-L-NC	304LB-L-WC	304LW-W	304LW-W-L-NC	304LW-W-L-WC
DOS, I_r/I_a	0.00003	0.00641	0.0002	0.00104	0.00614	0.00396
IGC rate, mm/y	0.12	0.46	0.52	0.2	0.46	0.3

Figure 7 shows the corroded grain boundaries in the cross-section of non-peened and peened 304L stainless steel after the immersion test for 15 h in boiling 65% HNO₃. In the case of 304L base metal, the grain boundaries were selectively corroded, regardless of the area. However, in the case of laser-peened specimens, the grain boundaries of the inside coarse grains were selectively corroded, although, the grain boundaries refined by laser peening were selectively corroded. Therefore, the intergranular corrosion rate of the laser-peened specimen was increased over that of the non-peened specimen. We recently reported the detrimental and beneficial effects of surface modification technology; in the case of non-sensitized 316L stainless steel, the effect of ultrasonic nano-crystal surface modification treatment on intergranular corrosion was detrimental, but this treatment on slightly sensitized 316L stainless steel showed a beneficial effect on intergranular corrosion. This behavior was due to reduced carbon segregation, grain refinement, and compressive residual stress [36].

3.2. Effect of Laser Peening on the Polarization Behavior of 304L Stainless Steel

Figure 8 shows the effect of laser peening on the polarization curves on the surface area of 304L stainless steel in deaerated 1% NaCl at 30 °C. Figure 8a shows that the transpassive potential of the 304L base metal was 0.985 V (SCE) and the stable passive current density was obtained, but the pitting potentials of the laser-peened 304LB-L-NC and 304LB-L-WC were 0.25 and 0.107 V (SCE), respectively. In the case of the HAZ area, the pitting potentials of the non-peened, peened without coating, and peened specimens with coating were 0.646, 0.056, and 0.402 V (SCE), respectively (Figure 8b). Moreover, in the case of weldment, the pitting potentials of the non-peened, peened without coating, and peened specimens with coating were 0.795, 0.086, and 0.268 V (SCE), respectively, as shown in Figure 8c. In summary, in the case of the polarization behavior of the surface, it is well known that the welding process reduces resistance due to sensitization and microstructural change [18]; laser peening decreased the pitting resistance, which was related to the surface roughness, as described elsewhere [18]. Irrespective of Al coating, the laser peening roughened the

surface [18], and a high static load in UNSM could degrade the corrosion resistance as a high static load and repeated process can create an overlapped wave [33].

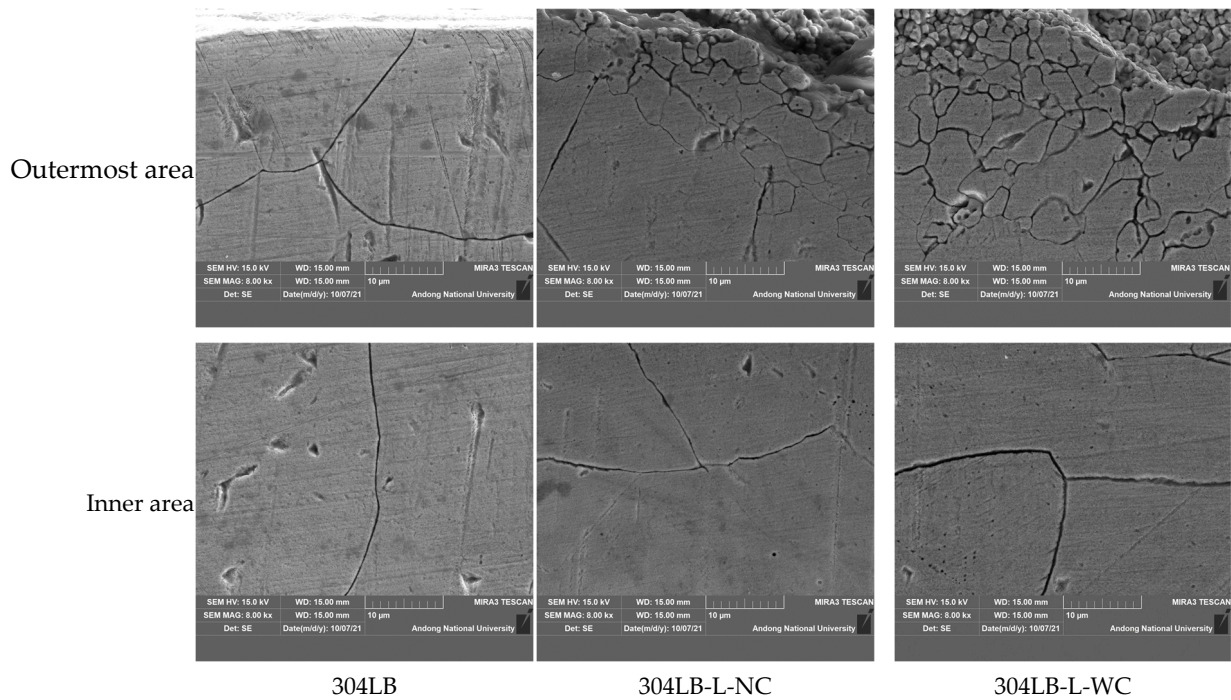


Figure 7. Corroded grain boundaries (SEM, $\times 8000$) in the cross-section of 304L stainless steel after the immersion test for 15 h in a boiling 65% HNO_3 .

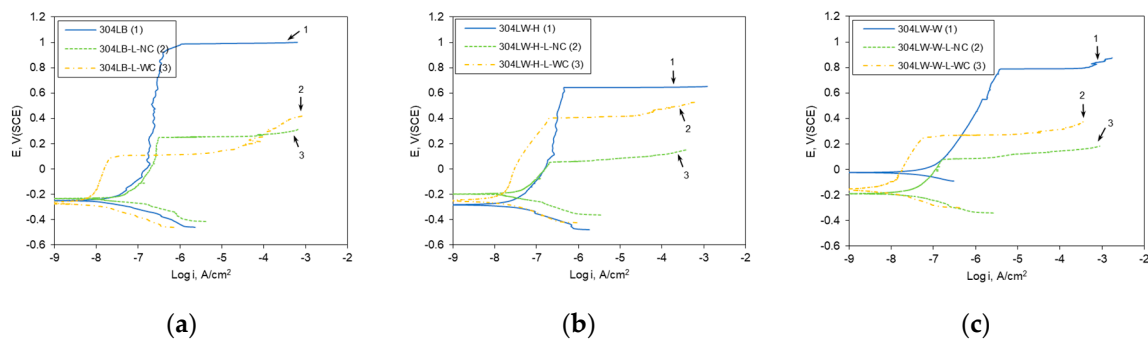


Figure 8. Effect of laser peening on the polarization curves of 304L-surface area (30 °C, deaerated 1% NaCl); (a) Base metal, (b) HAZ area, (c) Weldment.

Figure 9 shows the effect of laser peening on the polarization curves in the cross-sectional area of 304L in deaerated 1% NaCl at 30 °C. Figure 9a shows that the pitting potential of the 304L base metal was 0.212 V (SCE), but the pitting potentials of the laser-peened 304LB-L-NC and 304LB-L-WC were 0.23 and 0.428 V (SCE), respectively. Laser peening also reduced the passive current densities. In the case of the HAZ area, the pitting potentials of the non-peened, peened without coating, and peened specimens with coating were 0.222, 0.235, and 0.250 V (SCE), respectively, as in Figure 9b. Moreover, in the case of weldment, the pitting potentials of the non-peened, peened without coating, and peened specimens with coating were 0.065, 0.326, and 0.375 V (SCE), respectively, as shown in Figure 9c. In addition, laser peening decreased the passive current densities. In summary, laser peening on the outermost area of the cross-section of 304L stainless steel enhanced the polarization properties, irrespective of Al coating, which is related to the microstructural change by laser peening. As recently reported, laser peening refined the

grain size, deformed the inside, and increased the dislocation density [18]. Similar effects in UNSM-treated Alloy 600 were discussed [33].

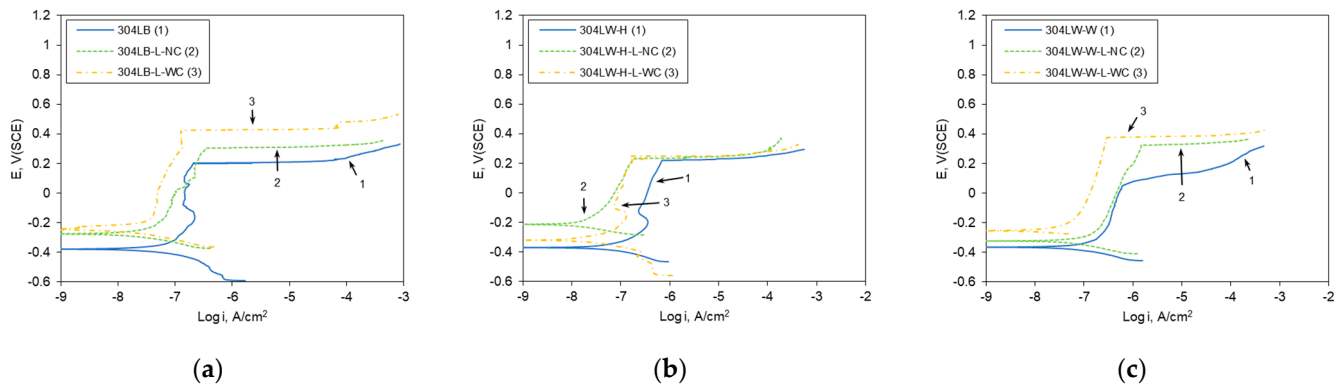


Figure 9. Effect of laser peening on the polarization curves of 304L-cross-section area (30 °C, deaerated 1% NaCl); (a) Base metal, (b) HAZ area, (c) Weldment.

The corrosion current density (i_R), corrosion potential (E_R), and pitting potential (E_P) of the surface and cross-section of 304L stainless steel are summarized in Tables 6 and 7, respectively. In the case of the surface, laser peening increased the corrosion current density and reduced the pitting potential, while laser peening decreased the corrosion current density and increased the pitting potential of the cross-section (corrosion current density was obtained through Tafel extrapolation analysis).

Table 6. The corrosion factors of the surface of 304L stainless steel obtained from Tafel extrapolation.

Surface Area	Non-Peened 304L			304L-L-NC			304L-L-WC		
	i_R , nA/cm ²	E_R , V(SCE)	E_P , V(SCE)	i_R , nA/cm ²	E_R , V(SCE)	E_P , V(SCE)	i_R , nA/cm ²	E_R , V(SCE)	E_P , V(SCE)
Base metal	12.28	−0.248	0.985	26.48	−0.232	0.25	4.03	−0.266	0.107
HAZ	11.91	−0.283	0.646	23.06	−0.197	0.056	5.83	−0.247	0.402
Weldment	24.34	−0.020	0.795	23.99	−0.188	0.086	3.29	−0.155	0.268

Table 7. The corrosion factors of the cross-section of 304L stainless steel obtained from Tafel extrapolation.

Cross-Section Area	Non-Peened 304L			304L-L-NC			304L-L-WC		
	i_R , nA/cm ²	E_R , V(SCE)	E_P , V(SCE)	i_R , nA/cm ²	E_R , V(SCE)	E_P , V(SCE)	i_R , nA/cm ²	E_R , V(SCE)	E_P , V(SCE)
Base metal	42.97	−0.378	0.212	17.94	−0.275	0.23	7.89	−0.245	0.428
HAZ	58.00	−0.367	0.222	10.33	−0.213	0.235	24.73	−0.317	0.250
Weldment	46.31	−0.364	0.065	44.82	−0.325	0.326	16.48	−0.252	0.375

Table 8 summarizes the residual stress measured on the surface and at 1 mm depth of 304L stainless steel via a hole drilling method: The surface and 1 mm depth of non-peened 304L stainless steel showed tensile residual stress, but compressive residual stress of the peened specimen was formed, regardless of measuring areas.

Table 8. Residual stress on the surface and at 1 mm depth of 304L stainless steel.

Residual Stress, MPa	Non-Peened 304L		304L-L-NC		304L-L-WC	
	Surface	1 mm-Depth	Surface	1 mm-Depth	Surface	1 mm-Depth
Base metal	92	14	−786	−128	−794	−131
HAZ	335	41	−497	−55	−565	−56
Weldment	11	119	−532	−118	−629	−229

Therefore, it can be elucidated that laser peening treatment can refine grain size [18] and induce compressive residual stress, thereby improving the passivation properties of 304L stainless steel. However, it should be noted that the pitting resistance of the surface by laser peening was reduced due to the increased irregularity including an overlapped surface and increased corrosion initiate sites by laser peening [34].

A comparison of the polarization curves of 304L stainless steel in Figures 8 and 9 shows that the pitting potentials of the cross-section were much lower than those of the surface. As the surface was rougher than the cross-section, this was an interesting result. Figure 10 shows the corrosion morphology of the cross-section after an anodic polarization test of 304LB. It was electrochemically etched using 10% oxalic acid solution. The optical micrograph (Figure 10a) shows the mechanical flow lines by the rolling process. An SEM micrograph (Figure 10b) shows the pits in the mechanical flow line area, including grain boundaries. Thus, the mechanical flow line formed by the rolling process seemed to act as the pitting initiation site and thus this flow reduces the pitting corrosion resistance of 304L stainless steel, as shown in Figure 10c.

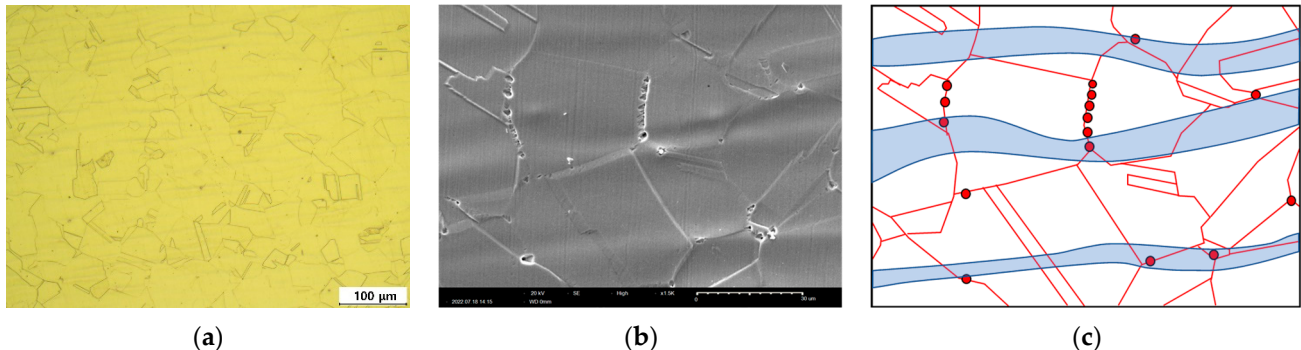


Figure 10. Corrosion morphologies of cross-section after anodic polarization test of 304LB (10% Oxalic acid, (a) OM ($\times 100$), (b) SEM ($\times 1500$)), and (c) schematic diagram (blue band is mechanical flow and red points are pits).

Figure 11 shows the effect of laser peening on the AC Impedance behavior of the cross-section of 304L stainless steel in deaerated 1% NaCl at 30 °C. The polarization resistance of the 304L base metal was 1230 k Ω , but the resistances of the laser-peened 304LB-L-NC and 304LB-L-WC were 2250 and 1800 k Ω , respectively. In the case of the HAZ area, the resistance of the non-peened specimen was 341 k Ω , but the resistances of the laser-peened 304LW-H-L-NC and 304LW-H-L-WC were 1070 and 1730 k Ω , respectively. In the case of the weldment area, the resistance of the non-peened specimen was 131 k Ω , but the resistances of the laser-peened 304LW-W-L-NC and 304LW-W-L-WC were 1900 and 1510 k Ω , respectively. In summary, regardless of base metal and welded areas, the laser peening enhanced the passive properties, and this was consistent with the above polarization test.

Author Contributions: Conceptualization, Y.-R.Y. and S.-H.C.; methodology, S.-H.C.; validation, Y.-R.Y.; investigation, S.-H.C.; data curation and analysis, Y.-R.Y.; writing—original draft preparation, Y.-R.Y. and S.-H.C.; writing—review and editing, Y.-R.Y. and Y.-S.K.; supervision, Y.-S.K. All authors have read and agreed to the published version of the manuscript.

Funding: This work was supported by a grant from the 2021–2022 Research Funds of Andong National University.

Institutional Review Board Statement: Not applicable.

Informed Consent Statement: Not applicable.

Data Availability Statement: Not applicable.

Acknowledgments: This research was also partly supported by the Korea Institute for Advancement of Technology (KIAT) grant funded by the Korea Government (MOTIE) (P0008458, HRD Program for Industrial Innovation, 2022).

Conflicts of Interest: The authors declare no conflict of interest.

References

1. Larry, J. *Welding and Metal Fabrication*, 3rd ed.; Delmar Cengage Learning: New York, NY, USA, 2012; pp. 1–15.
2. Farnsworth, S.R. *Welding for Dummies*, 3rd ed.; Wiley Publishing: New York, NY, USA, 2010; pp. 7–53.
3. Kim, J.H.; Lee, W.R.; Kim, T.G.; Cheong, S.K. Micro-shockwave measurement and evaluation of laser shock peening. *Trans. Korean Soc. Mech. Eng. B* **2011**, *35*, 1041–1046. [[CrossRef](#)]
4. Amini, S.; Kariman, S.A.; Teimouri, R. The effects of ultrasonic peening on chemical corrosion behavior of aluminum 7075. *Int. J. Adv. Manuf. Technol.* **2017**, *91*, 1091–1102. [[CrossRef](#)]
5. Ma, C.; Andani, M.T.; Qin, H.; Moghaddam, N.S.; Ibrahim, H.; Jahadkbar, A.; Amerinatanzi, A.; Ren, Z.; Zhang, H.; Doll, G.L.; et al. Improving surface finish and wear resistance of additive manufactured nickel-titanium by ultrasonic nano-crystal surface modification. *J. Mater. Process. Technol.* **2017**, *249*, 433–440. [[CrossRef](#)]
6. Tsai, W.T.; Chang, C.S.; Lee, J.T. Effects of shot peening on corrosion and stress corrosion cracking behaviors of sensitized alloy 600 in thiosulfate solution. *Corros. Sci.* **1994**, *50*, 98–105. [[CrossRef](#)]
7. Okimura, K.; Konno, T.; Narita, M.; Ohta, T.; Toyoda, M. Reliability of water jet peening as residual stress improvement method for alloy 600 PWSCC mitigation. In Proceedings of the International Conference on Nuclear Engineering, Orlando, FL, USA, 11–15 May 2008. [[CrossRef](#)]
8. Gujba, A.K.; Medraj, M. Laser Peening Process and Its Impact on Materials Properties in Comparison with Shot Peening and Ultrasonic Impact Peening. *Materials* **2014**, *7*, 7925–7974. [[CrossRef](#)] [[PubMed](#)]
9. Shiganov, I.N.; Misurov, A.I.; Melnikov, D.M. Laser shock peening of welded joints. *J. Phys. Conf. Ser.* **2018**, *1109*, 012018. [[CrossRef](#)]
10. Sadeh, S.; Malik, A. Investigation into the effects of laser shock peening as a post treatment to laser impact welding. *Mater. Des.* **2021**, *205*, 109701. [[CrossRef](#)]
11. Zhou, J.Z.; Huang, S.; Sheng, J.; Lu, J.Z.; Wang, C.D.; Chen, K.M.; Ruan, H.Y.; Chen, H.S. Effect of repeated impacts on mechanical properties and fatigue fracture morphologies of 6061-T6 aluminum subject to laser peening. *Mater. Sci. Eng. A* **2012**, *539*, 360–368. [[CrossRef](#)]
12. Huang, S.; Zhou, J.Z.; Sheng, J.; Lu, J.Z.; Sun, G.F.; Meng, X.K.; Zuo, L.D.; Ruan, H.Y.; Chen, H.S. Effects of laser energy on fatigue crack growth properties of 6061-T6 aluminum alloy subjected to multiple laser peening. *Eng. Fract. Mech.* **2013**, *99*, 87–100. [[CrossRef](#)]
13. Yella, P.; Venkateswarlu, P.; Buddu, R.K.; Vidyasagar, D.V.; Rao, K.B.S.; Kiran, P.P.; Rajulapati, K.V. Laser shock peening studies on SS316LN plate with various sacrificial layers. *Appl. Surf. Sci.* **2018**, *435*, 271–280. [[CrossRef](#)]
14. Gołrnikowska, M.R.; Kusiński, J.; Cieniek, Ł. Effect of laser shock peening on the microstructure and properties of the inconel 625 surface layer. *J. Mater. Eng. Perform.* **2020**, *29*, 1544–1549. [[CrossRef](#)]
15. Zhang, W.; Lu, J.; Luo, K. Residual stress distribution and microstructure at a laser spot of AISI 304 stainless steel subjected to different laser shock peening impacts. *Metals* **2016**, *6*, 6. [[CrossRef](#)]
16. Prabhakaran, S.; Kalainathan, S. Compound technology of manufacturing and multiple laser peening on microstructure and fatigue life of dual-phase spring steel. *Mater. Sci. Eng. A* **2016**, *674*, 634–645. [[CrossRef](#)]
17. Kumagai, M.; Curd, M.E.; Soyama, H.; Ungár, T.; Ribárik, G.; Withers, P.J. Depth-profiling of residual stress and microstructure for austenitic stainless steel surface treated by cavitation, shot and laser peening. *Mater. Sci. Eng. A* **2021**, *813*, 141037. [[CrossRef](#)]
18. Yoo, Y.R.; Kim, J.S.; Kim, Y.S. Effect of laser peening on microstructural changes in GTA-welded 304L stainless steel. *Materials* **2022**, *15*, 3947. [[CrossRef](#)]
19. Ye, Z.; Liu, D.; Li, C.; Zhang, X.; Yang, Z.; Lei, M. Effect of shot peening and plasma electrolytic oxidation on the intergranular corrosion behavior of 7A85 aluminum alloy. *Acta Metall. Sin.* **2014**, *27*, 705–713. [[CrossRef](#)]

20. Pandey, V.; Singh, J.K.; Chattopadhyay, K.; Srinivas, N.C.S.; Singh, V. Influence of ultrasonic shot peening on corrosion behavior of 7075aluminum alloy. *J. Alloy. Compd.* **2017**, *723*, 826–840. [[CrossRef](#)]
21. Lu, J.Z.; Qi, H.; Luo, K.Y.; Luo, M.; Cheng, X.N. Corrosion behaviour of AISI 304 stainless steel subjected to massive laser shock peening impacts with different pulse energies. *Corros. Sci.* **2014**, *80*, 53–59. [[CrossRef](#)]
22. Wang, T.; Yu, J.; Dong, B. Surface nano crystallization induced by shot peening and its effect on corrosion resistance of 1Cr18Ni9Ti stainless steel. *Surf. Coat. Technol.* **2006**, *200*, 4777–4781. [[CrossRef](#)]
23. Telang, A.; Gill, A.S.; Teyseyre, S.; Mannava, S.R.; Qian, D.; Vasudevan, V.K. Effects of laser shock peening on SCC behavior of Alloy 600 in tetrathionate solution. *Corros. Sci.* **2015**, *90*, 434–444. [[CrossRef](#)]
24. Gupta, R.K.; Kumar, B.S.; Sundar, R.; Sankar, P.R.; Ganesh, P.; Kaul, R.; Kain, V.; Ranganathan, K.; Bindra, K.S.; Singh, B. Enhancement of intergranular corrosion resistance of type 304 stainless steel through laser shock peening. *Corros. Eng. Sci. Technol.* **2017**, *52*, 220–225. [[CrossRef](#)]
25. Karthik, D.; Swaroop, S. Effect of laser peening on electrochemical properties of titanium stabilized 321 steel. *Mater. Chem. Phys.* **2017**, *193*, 147–155. [[CrossRef](#)]
26. Liu, D.; Shi, Y.; Liu, J.; Wen, L. Effect of laser shock peening on corrosion resistance of 316L stainless steel laser welded joint. *Surf. Coat. Technol.* **2019**, *378*, 124824. [[CrossRef](#)]
27. Kalainathan, S.; Sathyajith, S.; Swaroop, S. Effect of laser shot peening without coating on the surface properties and corrosion behavior of 316L steel. *Opt. Lasers Eng.* **2012**, *50*, 1740–1745. [[CrossRef](#)]
28. Lim, H.T.; Kim, P.K.; Jeong, H.M.; Jeong, S.H. Enhancement of abrasion and corrosion resistance of duplex stainless steel by laser shock peening. *J. Mater. Process. Technol.* **2012**, *212*, 1347–1354. [[CrossRef](#)]
29. Prabhakaran, S.; Kulkarni, A.; Vasanth, G.; Kalainathan, S.; Shukla, P.; Vasudevan, V.K. Laser shock peening without coating induced residual stress distribution, wettability characteristics and enhanced pitting corrosion resistance of austenitic stainless steel. *Appl. Surf. Sci.* **2018**, *428*, 17–30. [[CrossRef](#)]
30. Liu, P.; Sun, S.; Hu, J. Effect of laser shock peening on the microstructure and corrosion resistance in the surface of weld nugget zone and heat-affected zone of FSW joints of 7050 Al alloy. *Opt. Laser Technol.* **2019**, *112*, 1–7. [[CrossRef](#)]
31. Liu, H.; Tong, Z.; Zhou, W.; Yang, Y.; Jiao, J.; Ren, X. Improving electrochemical corrosion properties of AZ31 magnesium alloy via phosphate conversion with laser shock peening pretreatment. *J. Alloy. Compd.* **2020**, *846*, 155837. [[CrossRef](#)]
32. Martin, U.; Röss, J.; Bosch, J.; Bastidas, D.M. Evaluation of the DOS by DL–EPR of UNSM processed inconel 718. *Metals* **2020**, *10*, 204. [[CrossRef](#)]
33. Kim, K.T.; Kim, Y.S. The Effect of the static load in the UNSM process on the corrosion properties of alloy 600. *Materials* **2019**, *12*, 3165. [[CrossRef](#)] [[PubMed](#)]
34. Kim, K.T.; Kim, Y.S. Effect of the amplitude in ultrasonic nano-crystalline surface modification on the corrosion properties of alloy 600. *Corros. Sci. Technol.* **2019**, *18*, 196–205. [[CrossRef](#)]
35. Lee, J.H.; Kim, Y.S. Intergranular corrosion of 316L stainless steel by aging and UNSM (Ultrasonic Nano-crystal Surface Modification) treatment. *Corros. Sci. Technol.* **2015**, *14*, 313–324. [[CrossRef](#)]
36. Lee, J.H.; Kim, K.T.; Pyoun, Y.S.; Kim, Y.S. Intergranular corrosion mechanism of slightly-sensitized and UNSM-treated 316L stainless steel. *Corros. Sci. Technol.* **2016**, *15*, 226–236. [[CrossRef](#)]
37. Kim, K.T.; Lee, J.H.; Kim, Y.S. Effect of ultrasonic nano-crystal surface modification (UNSM) on the passivation behavior of aged 316L stainless steel. *Materials* **2017**, *10*, 713. [[CrossRef](#)] [[PubMed](#)]
38. Amanov, A. Effect of local treatment temperature of ultrasonic nanocrystalline surface modification on tribological behavior and corrosion resistance of stainless steel 316L produced by selective laser melting. *Surf. Coat. Technol.* **2020**, *398*, 126080. [[CrossRef](#)]
39. ASTM. A262-2002; Standard Practices for Detecting Susceptibility to Intergranular Attack in Austenitic Stainless Steels. ASTM International: West Conshohocken, PA, USA, 2002.
40. ASTM. G108-2004; Standard Test Method for Electrochemical Reactivation (EPR) for Detecting Sensitization of AISI Type 304 and 304L Stainless Steels. ASTM International: West Conshohocken, PA, USA, 2004.
41. ASTM. G5-2004; Standard Reference Test Method for Making Potentiostatic and Potentiodynamic Anodic Polarization Measurements. ASTM International: West Conshohocken, PA, USA, 2004.
42. ASTM G3-2004; Standard Practice for Conventions Applicable to Electrochemical Measurements in Corrosion Testing. ASTM International: West Conshohocken, PA, USA, 2004.
43. ASTM E1382; Standard Test Method for Determining Average Grain Size Using Semiautomatic and Automatic Image Analysis. ASTM International: West Conshohocken, PA, USA, 2015.
44. ISO 12732-2006; Electrochemical Potentiokinetic Reactivation Measurement Using the Double Loop Method. ISO: Geneva, Switzerland, 2006.

Disclaimer/Publisher’s Note: The statements, opinions and data contained in all publications are solely those of the individual author(s) and contributor(s) and not of MDPI and/or the editor(s). MDPI and/or the editor(s) disclaim responsibility for any injury to people or property resulting from any ideas, methods, instructions or products referred to in the content.